

# Mineral-hosted biofilm communities in the continental deep subsurface, Deep Mine Microbial Observatory, SD, USA

Caitlin P. Casar<sup>1</sup>, Brittany R. Kruger<sup>3</sup>, Theodore M. Flynn<sup>2</sup>, Andrew L. Masterson<sup>1</sup>, Lily Momper<sup>1</sup>, Magdalena R. Osburn<sup>1</sup>, Jan Amend<sup>4</sup>

<sup>1</sup>Northwestern University, Department of Earth and Planetary Sciences, Evanston IL, 60208

<sup>2</sup>Argonne National Laboratory, Argonne IL

<sup>3</sup>Desert Research Institute, Division of Hydrologic Sciences, Las Vegas NV, 89113

<sup>4</sup>University of Southern California, Los Angeles CA, 90007

## Abstract

Deep subsurface biofilms are estimated to host the majority of prokaryotic life on Earth yet, fundamental aspects of their ecology remain unknown (Flemming and Wuertz, 2019). An inherent difficulty in studying subsurface biofilms that of sampling. While, samples from marine and terrestrial deep subsurface fracture and pore fluids systems have revealed abundant and diverse microbial life, limited recent work has described the corresponding biofilms on rock fracture and pore space surfaces. The recently established Deep Mine Microbial Observatory is a long-term monitoring station at which we can explore the role of biofilms in fluid-filled fractures to depths of 4,850 ft. ...

## 1 | INTRODUCTION

The continental deep subsurface biosphere extends to great depths in the Earth's crust, ending only where temperature, pressure, water limitation, or pore size preclude life (Rebata-Landa & Santamarina, 2006; Hazael *et al.*, 2016). The conditions found within these deep environments pose distinct biological challenges, particularly a lack of photosynthetic energy and limited organic carbon. Despite these challenges, microbial life has been and has been detected as deep as 2.8km (Chivian *et al.*, 2008) and is comprised of as many as  $3 \times 10^{29}$  cells, or 30% of global prokaryotic biomass (Magnabosco *et al.*, 2018; Flemming & Wuertz, 2019). Fluid-filled fractures serve as oases for microbial life where interactions between the host rock and fracture fluids provide abundant insoluble and dissolved electron donors and acceptors, establishing chemical disequilibrium that can support chemolithotrophic microbial metabolisms. Although the relative importance of chemolithotrophs specifically is unknown, they may constitute a large percentage of this vast biosphere given the limited availability of organic carbon. Genomic and metagenomic surveys support this assertion, revealing highly diverse biospheres with strong chemolithotrophic metabolic potential (i.e. Osburn *et al.*, 2014; Magnabosco *et al.*, 2016; Probst *et al.*, 2018). One significant caveat to these studies is that the majority of cell density estimates and sequence-based diversity measures are obtained from microbial communities filtered from fluids, thus missing a potentially significant contribution from communities attached to surfaces as biofilms. This potential significance is underscored by recent estimates of biofilm biomass in the continental subsurface, totaling as many as  $2.4 \times 10^{29}$  cells, or 80% of all continental deep subsurface biomass (Flemming & Wuertz, 2019).

Biofilm communities inhabiting the continental deep subsurface have been previously investigated using both laboratory-based (Thomas-Keprra *et al.*, 1998) and *in situ* cultivation approaches (Moser *et al.*, 2003; Lehman *et al.*, 2004; Henneberger *et al.*, 2006). These studies were among the first to identify the potential importance of attached communities in the deep biosphere, noting the potential for significant diversity and biomass in biofilm communities. Direct observations of South African biofilms on pristine fracture surfaces and within *in situ* incubation experiments estimated cell densities ranging from  $5 \times 10^4$  to  $3.4 \times 10^6$  cells/mm<sup>2</sup> (Moser *et al.*, 2003; Wanger *et al.*, 2006). Compared to the relatively low cell densities estimated

from the contemporaneous fracture fluids, high biofilm cell densities suggested a competitive advantage to biofilm formation under oligotrophic conditions. Biofilm colonization may be promoted by concentration of nutrients on rock surfaces via adsorption of hydrophobic molecules such as fatty acids (Marshall, 1988) or adsorption of cations (Prakash *et al.*, 2003). Further, the biofilm matrix itself can adsorb nutrients, as well as enhance nutrient recycling from lysed cells in the biofilm matrix, promote synergetic cell-to-cell interactions, and promote evolutionary advantage via gene exchange (Flemming *et al.*, 2016). Additionally, biofilm formation can promote extracellular electron transfer (EET) between cells and mineral surfaces via direct contact or EET mediators in the biofilm matrix (Lies *et al.*, 2005), and the potential for microbially-mediated metal reduction in the South African incubation experiments was indicated by geochemical modelling and PLFA profiles (Moser *et al.*, 2003). Finally, biofilms can host communities that differ in biodiversity and metabolic potential from suspended communities. A study comparing native communities in a basalt aquifer revealed significantly greater metabolic richness in suspended vs. rock-attached communities, and *in situ* cultivation experiments using dialysis chambers comparing these community types revealed differences in microbial community compositions (Lehman *et al.*, 2004). Importantly, the early findings from Moser *et al.*, 2003; Lehman *et al.*, 2004; and Wanger *et al.*, 2006 suggest that the commonly accepted practice of reporting diversity of planktonic sequencing campaigns misses significant differences between the distinct planktonic and attached populations. These findings warrant further studies to assay the ecological drivers of biodiversity and biomass in attached and suspended communities, and the metabolic relationships between biofilm community members and their attachment surfaces in the continental subsurface.

The Deep Mine Microbial Observatory (DeMMO) in the former Homestake Gold Mine in Lead, South Dakota, USA, is a recently established long-term monitoring station at which the ecology of the deep continental subsurface can be explored. DeMMO offers convenient access to fracture fluids emanating from a variety of continental rock types spanning depths of 250 to 1500 m, and is monitored for fluid chemistry and microbial diversity over time (Osburn *et al.*, 2019a, Osburn 2019b *in prep*). DeMMO includes six legacy boreholes that intersect fluid-filled fractures where each borehole has been adapted for periodic fluid sampling and instillation of long-term experiments with minimal disturbance to the fracture fluids. Long-term monitoring of fracture fluids here has revealed stable fluid chemistry since December 2015 and limited disturbance to the system associated with borehole modification (Osburn *et al.*, 2019a). Genomic and metagenomic surveys of microbial communities captured from fracture fluids indicate the presence of distinct microbial assemblages at each DeMMO site, locally dominated by candidate phyla and unclassified taxa, that appear to be strongly influenced by fluid geochemistry (Osburn 2019b *in prep*, Momper *et al.* 2019 *in prep*).

DeMMO presents a unique opportunity for long-term *in situ* cultivation experiments, following methods from previous studies (i.e. Moser *et al.*, 2003; Lehman *et al.*, 2004), to specifically query the ecology of the attached fraction of the deep continental biosphere. A first order question is how different are the taxonomic compositions of fluid and biofilm communities? While previous studies suggest potential major differences are possible (Lehman *et al.*, 2004; Lehman, 2007), it is thus far unclear if this is a universal phenomenon. Further, a variety of minerals in the surrounding host rock are available as energy sources, and metabolic reactions using some of these minerals were previously found to be thermodynamically favorable at DeMMO (Osburn *et al.*, 2014). However, the relationship between the biofilm communities and potential mineral-based metabolisms remains unexplored. Finally, mineral selectivity by microbes has been observed (Murr & Berry, 1976; Lawrence *et al.*, 1997), but identifying the specific taxa and amount of biomass a given mineral type supports in continental deep subsurface environments has not previously attempted. By comparing fluid and biofilm communities and exploring relationships between biofilms and available

minerals in the surrounding host rock, we aim to constrain controls on biodiversity and biomass in the continental deep biosphere. Here, we describe an *in situ* cultivation-based approach designed to probe the microbial ecology of mineral-hosted biofilms inhabiting fluid-filled fractures at DeMMO.

## 2 | MATERIALS AND METHODS

### 2.1 | DeMMO

DeMMO is located within the former Homestake Gold Mine, Lead, SD, USA situated in an uplifted, deformed region of Paleoproterozoic metasediments and Tertiary igneous intrusions (Caddey *et al.*, 1991). The former mine, now known as the Sanford Underground Research Facility (SURF), is approximately 3.5 km wide and is currently accessible to a depth of 1.5 km; however, previous mining operations extended to a depth of 2.5 km (Figure 1). The mining levels intersect the Ellison, Homestake, and Poorman formations. The Ellison Formation is comprised of pelitic phyllite and interbedded quartzite. The Homestake Formation is gold ore-bearing, carbonate-rich iron formation. The upper Poorman Formation is composed primarily of graphitic phyllite locally rich in iron sulfides and large quartz veins overlaying a lower unit of metabasalt (Yates Unit) (Caddey *et al.*, 1991). The shallow levels and those near to the mine workings capture relatively young fluids that are recharged on annual timescales by meteoric water, whereas deeper sites capture fluids from a regional flow system that have estimated residence times on the order of 10,000 years or greater (Murdoch *et al.*, 2012).

Fracture fluids at sites DeMMO1, DeMMO3, and DeMMO6, hereafter referred to as D1, D3, and D6, are geochemically (Table 1) and taxonomically distinct (Osburn *et al.*, 2019a, Osburn 2019b *in prep*). D1 is located at a depth of 800 feet, and fluids are moderately reducing with high concentrations of dissolved ferrous iron, dominated by candidate phylum *Omnitrophica* and unclassified taxa. D3 is located at a depth of 2,000 feet, with ferrous iron and sulfate-rich suboxic fluids dominated by members of *Betaproteobacteria* and *Nitrospirae*. D6 is located at a depth of 4,850 feet, with reducing, sulfate and methane-rich fluids dominated by members of *Deltaproteobacteria* and *Firmicutes*. All three of these sites are drilled away from the mine workings and likely have significant water residence times.

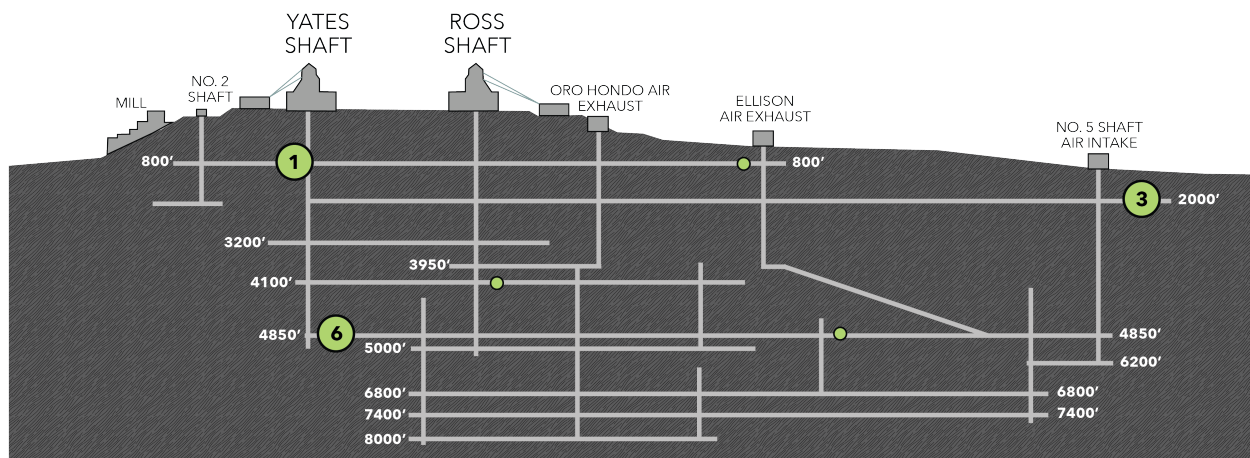


**Figure 1.** Cross-sectional view of the Deep Mine Microbial Observatory (DeMMO). Grey lines are tunnels and shafts in the mine. Green circles represent locations of six DeMMO sites, larger circles represent the three sites in this study: D1, D3, and D6.

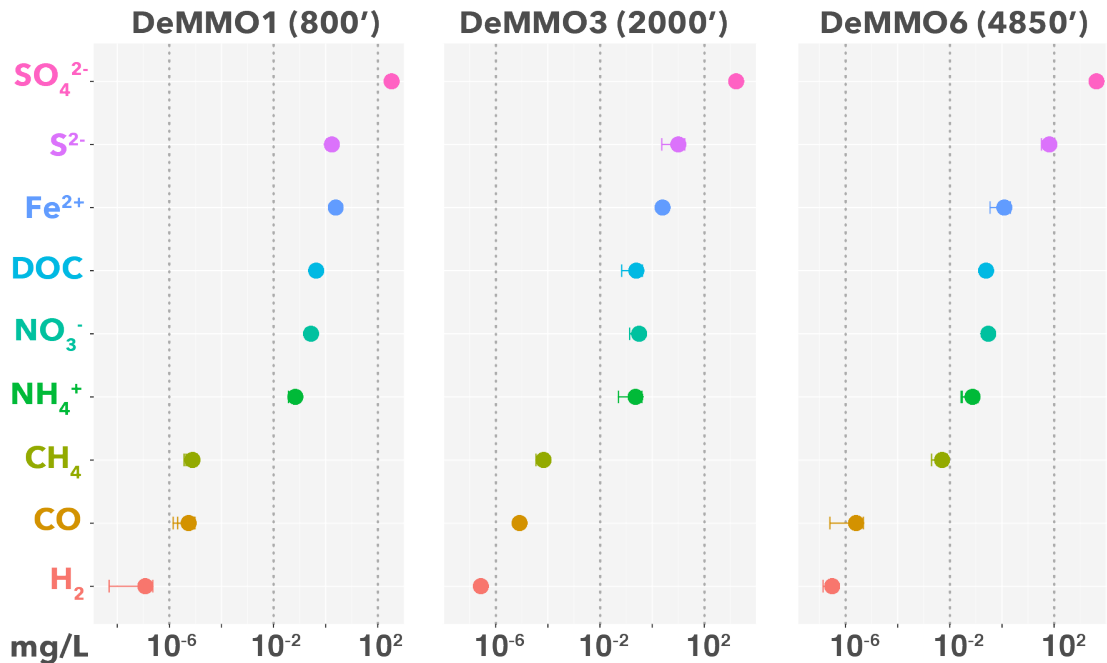


Figure 2. Averaged fracture fluid chemistry at DeMMO measured between December 2015-April 2018.

## 2.2 | Thermodynamic Modeling of Microbial Metabolisms

To investigate the metabolic potential of biofilm communities, we modeled 39 reactions with minerals under *in situ* conditions at DeMMO (Figure 2). We collected DeMMO fluid geochemical data 11 times between December 2015 and September 2018 (Osburn *et al.*, 2019a). This robust geochemical record was used to generate averaged fluid chemistries for D1, D3, and D6 (Table 1) used in species activity calculations via SPECE8 in Geochemist's Workbench (Bethke *et al.*, 2009). Species activities and average fluid temperatures were used to calculate activity and equilibrium constants for each metabolic reaction in CHNOSZ (Dick, 2008). Finally, Gibbs energy yields ( $G_r$ ) and energy densities ( $E_r$ ) of each reaction were calculated following the methods of Osburn *et al.*, 2014 (equations 1-3).

**Table 2.** Metabolic reactions with minerals in this study.

No.	Reaction	e-/rxn	No.	Reaction	e-/rxn			
<b>Pyrolusite as electron acceptor</b>								
1	$MnO_2 + H_2 + 2H^+ \leftrightarrow Mn^{2+} + 2H_2O$	2	23	$CaSO_4 \cdot 2H_2O + CH_3COO^- \leftrightarrow HS^- + 2HCO_3^- + Ca^{2+} + 2H_2O$	8			
2	$MnO_2 + HS^- + 2H^+ \leftrightarrow Mn^{2+} + S^0 + 2H_2O$	2	24	$CaSO_4 \cdot 2H_2O + 8Mn^{2+} + 10H_2O \leftrightarrow HS^- + 8MnOOH + Ca^{2+} + 15H^+$	8			
3	$3MnO_2 + NH_4^+ + 4H^+ \leftrightarrow 3Mn^{2+} + NO_2^- + 4H_2O$	6	25	$CaSO_4 \cdot 2H_2O + 4CO + 2H_2O \leftrightarrow 4HCO_3^- + HS^- + Ca^{2+} + 3H^+$	8			
4	$MnO_2 + CH_4 + 7H^+ \leftrightarrow 4Mn^{2+} + HCO_3^- + 5H_2O$	8	<b>Siderite as electron donor</b>					
5	$MnO_2 + Fe^{2+} + 2H_2O \leftrightarrow Mn^{2+} + 2FeOOH + 2H^+$	2	26	$2FeCO_3 + NO_3^- + 3H_2O \leftrightarrow 2FeOOH + NO_2^- + 2HCO_3^- + 2H^+$	2			
6	$3MnO_2 + S^0 + 4H^+ \leftrightarrow 3Mn^{2+} + SO_4^{2-} + 2H_2O$	6	27	$8FeCO_3 + SO_4^{2-} + 12H_2O \leftrightarrow 8FeOOH + HS^- + 8HCO_3^- + 7H^+$	8			
			28	$6FeCO_3 + CO + 11H_2O \leftrightarrow 6FeOOH + 6HCO_3^- + CH_4 + 6H^+$	6			

7	$9\text{MnO}_2 + 2\text{CH}_3\text{COO}^- + 18\text{H}^+ \leftrightarrow 9\text{Mn}^{2+} + 4\text{HCO}_3^- + 10\text{H}_2\text{O}$	18	<b>Hematite as electron acceptor</b>		
8	$\text{MnO}_2 + \text{CO} + \text{H}^+ \leftrightarrow \text{Mn}^{2+} + \text{HCO}_3^-$	2			
<b>Magnetite as electron acceptor</b>					
9	$\text{Fe}_3\text{O}_4 + \text{H}_2 + 6\text{H}^+ \leftrightarrow 3\text{Fe}^{2+} + 4\text{H}_2\text{O}$	2	29	$\text{Fe}_2\text{O}_3 + \text{H}_2 + 4\text{H}^+ \leftrightarrow 2\text{Fe}^{2+} + 3\text{H}_2\text{O}$	4
10	$\text{Fe}_3\text{O}_4 + \text{HS}^- + 7\text{H}^+ \leftrightarrow 3\text{Fe}^{2+} + \text{S}^0 + 4\text{H}_2\text{O}$	2	30	$\text{Fe}_2\text{O}_3 + \text{HS}^- + 5\text{H}^+ \leftrightarrow 2\text{Fe}^{2+} + \text{S}^0 + 3\text{H}_2\text{O}$	2
11	$3\text{Fe}_3\text{O}_4 + \text{NH}_4^+ + 16\text{H}^+ \leftrightarrow 9\text{Fe}^{2+} + \text{NO}_2^- + 10\text{H}_2\text{O}$	6	31	$3\text{Fe}_2\text{O}_3 + \text{NH}_4^+ + 10\text{H}^+ \leftrightarrow 6\text{Fe}^{2+} + \text{NO}_2^- + 7\text{H}_2\text{O}$	6
12	$4\text{Fe}_3\text{O}_4 + \text{CH}_4 + 23\text{H}^+ \leftrightarrow 16\text{Fe}^{2+} + \text{HCO}_3^- + 13\text{H}_2\text{O}$	8	32	$4\text{Fe}_2\text{O}_3 + \text{CH}_4 + 15\text{H}^+ \leftrightarrow 8\text{Fe}^{2+} + \text{HCO}_3^- + 9\text{H}_2\text{O}$	8
13	$3\text{Fe}_3\text{O}_4 + \text{S}^0 + 16\text{H}^+ \leftrightarrow 9\text{Fe}^{2+} + \text{SO}_4^{2-} + 8\text{H}_2\text{O}$	6	33	$3\text{Fe}_2\text{O}_3 + \text{S}^0 + 10\text{H}^+ \leftrightarrow 6\text{Fe}^{2+} + \text{SO}_4^{2-} + 5\text{H}_2\text{O}$	6
14	$3\text{Fe}_3\text{O}_4 + 2\text{CH}_3\text{COO}^- + 6\text{H}^+ \leftrightarrow 9\text{Fe}^{2+} + 4\text{HCO}_3^- + 4\text{H}_2\text{O}$	18	34	$4\text{Fe}_2\text{O}_3 + \text{CH}_3\text{COO}^- + 15\text{H}^+ \leftrightarrow 8\text{Fe}^{2+} + 2\text{HCO}_3^- + 8\text{H}_2\text{O}$	8
15	$\text{Fe}_3\text{O}_4 + 2\text{Mn}^{2+} + 2\text{H}^+ \leftrightarrow 3\text{Fe}^{2+} + 2\text{MnOOH}$	6	35	$\text{Fe}_2\text{O}_3 + 2\text{Mn}^{2+} + \text{H}_2\text{O} \leftrightarrow 2\text{Fe}^{2+} + 2\text{MnOOH}$	2
16	$\text{Fe}_3\text{O}_4 + \text{CO} + 5\text{H}^+ \leftrightarrow 3\text{Fe}^{2+} + \text{HCO}_3^- + 2\text{H}_2\text{O}$	2	36	$\text{Fe}_2\text{O}_3 + \text{CO} + 3\text{H}^+ \leftrightarrow 2\text{Fe}^{2+} + \text{HCO}_3^- + \text{H}_2\text{O}$	2
<b>Gypsum as electron acceptor</b>					
17	$\text{CaSO}_4 \cdot 2\text{H}_2\text{O} + 4\text{H}_2 + \text{H}^+ \leftrightarrow \text{HS}^- + \text{Ca}^{2+} + 6\text{H}_2\text{O}$	8	37	$\text{FeS}_2 + 8\text{NO}_3^- \leftrightarrow \text{Fe}^{2+} + 2\text{SO}_4^{2-} + 8\text{NO}_2^-$	16
18	$\text{CaSO}_4 \cdot 2\text{H}_2\text{O} + 3\text{HS}^- + 5\text{H}^+ \leftrightarrow \text{S}^0 + \text{Ca}^{2+} + 6\text{H}_2\text{O}$	8	38	$\text{FeS}_2 + 2\text{HCO}_3^- + 2\text{H}_2\text{O} + 2\text{H}^+ \leftrightarrow \text{Fe}^{2+} + 2\text{SO}_4^{2-} + 2\text{CH}_4$	16
19	$3\text{CaSO}_4 \cdot 2\text{H}_2\text{O} + 4\text{NH}_4^+ \leftrightarrow 3\text{HS}^- + 4\text{NO}_2^- + 3\text{Ca}^{2+} + 10\text{H}_2\text{O} + 5\text{H}^+$	24	39	$3\text{FeS}_2 + 8\text{CO} + 16\text{H}_2\text{O} \leftrightarrow 3\text{Fe}^{2+} + 6\text{SO}_4^{2-} + 8\text{CH}_4$	48
20	$\text{CaSO}_4 \cdot 2\text{H}_2\text{O} + \text{CH}_4 \leftrightarrow \text{HCO}_3^- + \text{HS}^- + \text{Ca}^{2+} + 3\text{H}_2\text{O}$	8	* Aqueous forms were used for H <sub>2</sub> , CO, and CH <sub>4</sub>		
21	$\text{CaSO}_4 \cdot 2\text{H}_2\text{O} + 8\text{Fe}^{2+} + 10\text{H}_2\text{O} \leftrightarrow \text{HS}^- + 8\text{FeOOH} + \text{Ca}^{2+} + 15\text{H}^+$	8	** FeOOH and MnOOH are ferrihydrite and manganite, respectively		
22	$3\text{CaSO}_4 \cdot 2\text{H}_2\text{O} + 4\text{S}^0 \leftrightarrow 4\text{SO}_4^{2-} + 3\text{HS}^- + 5\text{H}^+ + 3\text{Ca}^{2+} + 2\text{H}_2\text{O}$	24	*** DOC concentrations were used to estimate acetate.		

## 2.3 | *In situ* Cultivation Experiments

We deployed *in situ* cultivation experiments to grow biofilm communities on minerals present in DeMMO host rock (Figure 3). Arrays of flow-through colonization reactors were filled with crushed and polished minerals (pyrite, hematite, magnetite, siderite, pyrolusite, muscovite, gypsum, and calcite) or inert control substrates (glass beads, glass wool, and sand). Crushed minerals were mixed with sand to a ratio of ~1:2 to minimize major changes in pH. The reactors were connected to borehole outflows at D1, D3, and D6 for 2–8 months to allow for colonization by biofilm communities prior to harvesting. After incubation, crushed mineral or inert control material was collected in sterile tubes and frozen on dry ice in the field for DNA. Additionally, we collected ~1L of fracture fluids on 0.2µm sterivex filters from each site for comparison of DNA from biofilm communities to fracture fluid communities. To control for the mine environment, we extracted DNA from standing water present in mine tunnels and from pre-sterilized glass slides incubated in open air in the mine tunnels for 2 months at depths of 800 and 4,100 feet. Polished mineral coupons or glass slides were included within each reactor for microscopy. Mineral coupons and glass slides were fixed in 4% glutaraldehyde in the field and stored at 4°C (except for gypsum coupons which were not recovered due to dissolution). Raw borehole fluids were also collected for enumeration by epifluorescence microscopy in sterile PET bottles and fixed with 4% paraformaldehyde in the field (Osburn 2019b *in prep*).

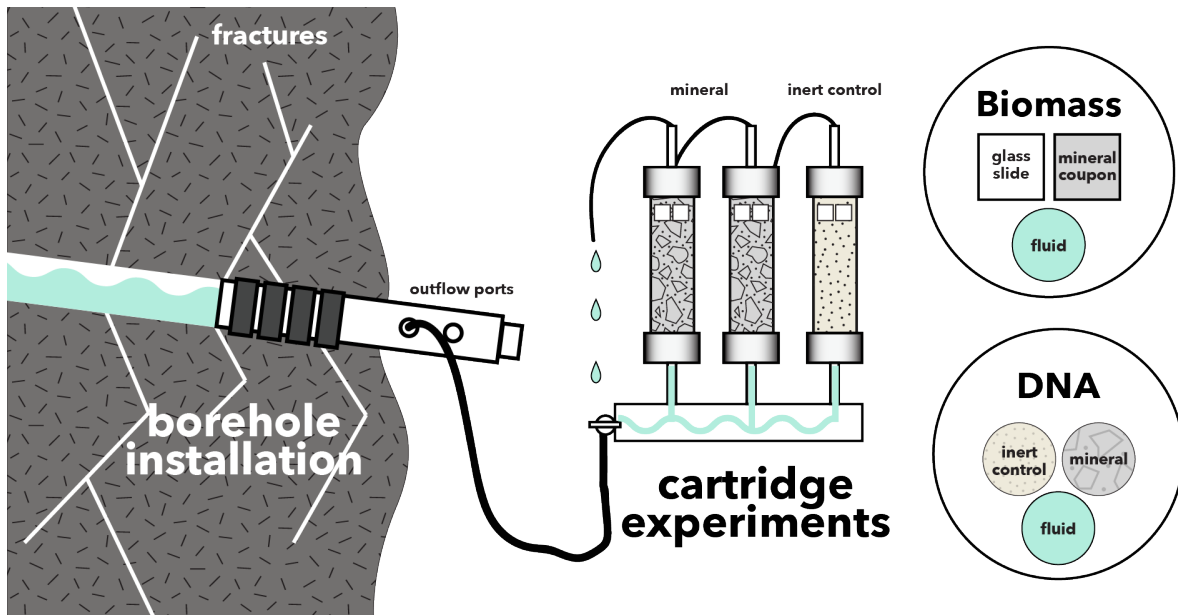


**Figure 3.** Fracture fluids flow from borehole installation sampling ports through cartridges filled with minerals or inert material. Glass slides and mineral coupons were included in the experiments for SEM to estimate biomass. DNA was sampled from fluids and cartridge materials to characterize microbial communities.

## 2.4 | Microbial Community Analysis

We extracted DNA from crushed mineral, inert control, and glass slide ambient background control samples using a MoBIO PowerBiofilm DNA Isolation Kit (Cat. No. 24000-50) and from Sterivex filters using a MoBIO PowerWater Sterivex DNA Isolation Kit (Cat No. 14600-50-NF) following the manufacturer suggested protocol. Whole genomic DNA was sent to Argonne National Laboratory for 16S rRNA amplicon sequencing of the V4 hypervariable region using 516F (GTGYCAGCMGCCGCGTAA) and 806R (GGACTACNVGGGTWTCTAAT) universal primers. Samples were sequenced on an Illumina MiSeq instrument. Paired-end reads were joined with PEAR (Zhang *et al.*, 2014) and demultiplexed with QIIME (v 1.9.1; Caporaso *et al.*, 2010). We acknowledge the growing trend of binning sequences into amplicon sequence variants (ASV's); however, we characterize microbial communities to the family level and are not attempting to assign strain-level taxonomy to sequences here. Further, alpha and beta diversity metrics were found to be highly correlated when comparing ASV and OTU binning of environmental 16S rRNA gene sequences resulting in ecologically similar interpretations between both approaches (Glassman & Martiny, 2018), thus we bin sequences into operational taxonomic units (OTU's). Sequences were dereplicated and binned into OTU's at a threshold similarity of 97%, and chimeric sequences were removed using USEARCH (Edgar, 2013). Rarefied OTU tables were generated in QIIME by randomly sampling sequences between read depths of 0 – 32,500, the approximate median value of total sequence reads among samples, at a step size of 500 and 10 permutations. Rarefaction curves were generated using the averages of the 10 permutations. We normalized the final OTU table for statistical analyses to a depth of 10,000 reads where rarefaction curves began to level off, indicating the read depth sufficiently captured alpha diversity among all samples. Representatives from each OTU were assigned taxonomy using the UCLUST method in QIIME referencing the SILVA132 database (Quast *et al.*, 2012). OTU's that were classified as "Unassigned" using the SILVA132 database were compared to DeMMO metagenome assembled genomes (MAG's) (Momper *et al.* 2019 *in prep*). In brief, reconstructed 16S genes were pulled from MAG's and were used as a Basic Local Alignment Search Tool (BLAST) database against which to query the

representative sequence from unassigned OTUs. Phylogenetic identities of MAGs were assigned using the Genome Taxonomy Database and the associated GTDB-Tk toolkit (Chaumeil et al, *in prep*). MAGs were queried for a putative 16S rRNA gene using the “ssu\_finder” command in the CheckM pipeline (Parks et al., 2015). All putative 16S genes longer than 300 bp from a single DeMMO site were compiled into a single file for that site. Each file was used to create a Standalone BLAST database (version 2.9.0) for that DeMMO site. Representative sequences from unassigned OTUs from each DeMMO sample were queried against their respective database with a minimum -evalue of  $10^{-10}$ . If a representative OTU sequence matched a MAG’s reconstructed 16S gene, the taxonomic assignment given to the MAG was also given to that OTU. When a single representative OTU sequence returned a hit for more than one MAG, the sequence with the lower evalue and better alignment was determined to be the appropriate assignment. More detailed methods and MAG sequences can be found in (Momper et al. 2019 *in prep*).

We performed statistical analyses on the rarefied OTU table using QIIME and the Vegan (Oksanen et al., 2019) and Ecodist (Goslee & Urban, 2007) packages in R. Alpha diversity was calculated using QIIME in terms of species richness (number of observed OTUs), evenness (Chao1 and Simpson), and diversity (Simpson, Faith’s, and Shannon). To illustrate beta diversity among DeMMO communities, we visualized DeMMO communities with stacked bar plots illustrating OTU community composition binned at the family level. Families that comprised less than 5% of communities we binned as “Less Abundant Taxa”. To further illustrate beta diversity using our entire dataset of DeMMO communities including all replicates and controls, we performed nonmetric multidimensional scaling (NMDS) with Vegan on communities at the OTU level using the metaMDS function Bray-Curtis metric with default parameters and a dimension size of 2. We used NCBI BLAST to search for the closest relatives of OTUs of interest (blast.ncbi.nlm.nih.gov).

## 2.5 | Microbial Cell Density Estimates

We documented cell morphologies and estimated cell densities on mineral coupons and inert glass slides from 1,300 scanning electron micrographs. Samples were gradually dehydrated in 200 proof ethanol and subjected to critical point drying to preserve cell structure. Coupons and slides were coated with osmium tetroxide to a thickness of 15nm to enhance sample conductivity for imaging on a FEI Quanta 650 environmental scanning electron microscope (SEM) in the EPIC facility at the Northwestern University NUANCE center. Images were collected using an operating voltage of 20 kV, 0.98 torr pressure, and working distance of ~5mm. We collected 20 images from each sample and counted cells from a minimum of either 300 cells or 10 images. In some cases, cells were counted from all 20 images and totaled less than 300 cells. To estimate planktonic cell densities, fixed fluids were filtered onto black polycarbonate filters, stained with DAPI (4’,6-diamidino-2-phenylindole) for ten minutes, and mounted on glass slides with Citifluor antifade reagent before visualizing with a Zeiss Axioscope 2 (Osburn 2019b *in prep*). Fracture fluid cell densities were converted from cells/mL to cells/cm<sup>2</sup> by assuming a conservative fracture width of 100µm (Wanger et al., 2006).

## 3 | RESULTS

### 3.1 Gibb’s free energy and energy density of metabolic reactions with minerals

We modeled 39 reactions, which range from highly endergonic, +105 kJ/mole e<sup>-</sup> transferred, to highly exergonic, -89 kJ/mole e<sup>-</sup> transferred ([Figure 3](#)). Of the 23 exergonic reactions, the most exergonic reaction is pyrite oxidation with nitrate, followed all pyrolusite reduction reactions and siderite oxidation with nitrate. All other reactions yielded little to no Gibb’s free energy or were endergonic.

In terms of energy density, carbon monoxide is most exergonic of dissolved reactants. Moderately exergonic reactants include nitrate, acetate, ferrous iron, methane, and sulfide, and hydrogen is the least exergonic reactant.

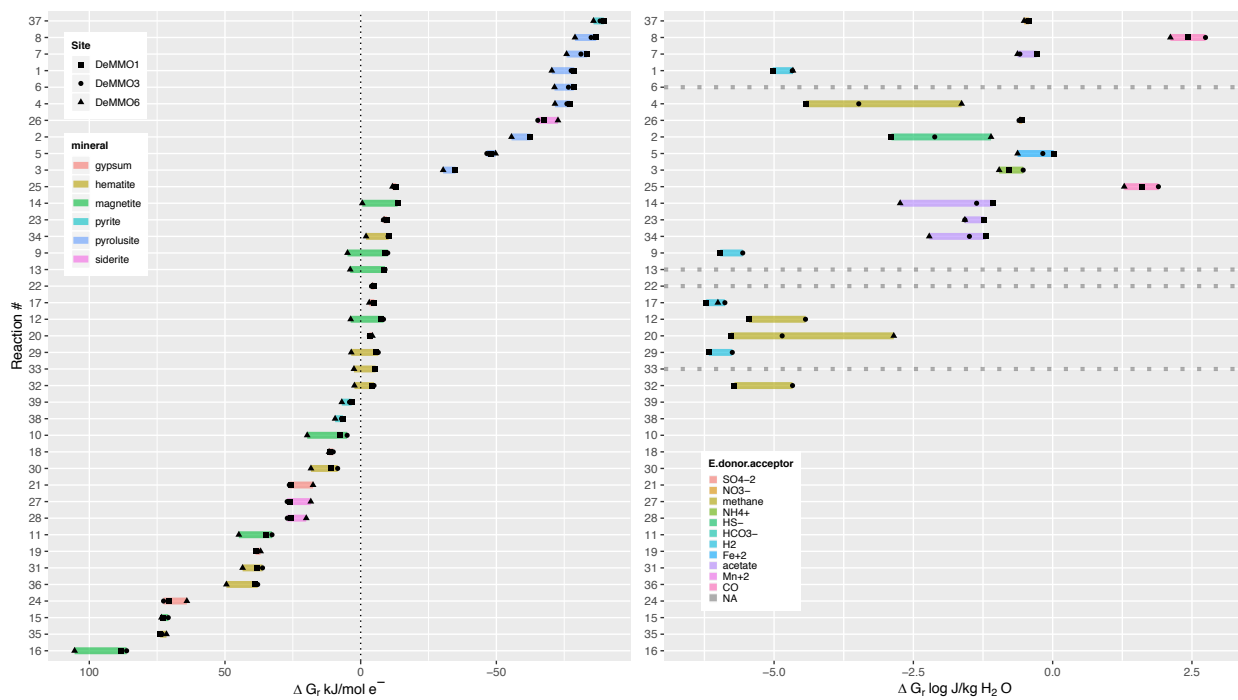


**Figure 3.** Free energy (left) and energy density (right) of reactions with minerals and dissolved electron donors and acceptors based on *in situ* geochemistry.

### 3.2 Microbial Communities

DeMMO fluid and biofilm communities include 7,015 OTU's (845 families from 66 phyla) after quality filtering and read depth normalization. On average, all communities are highly uneven, fluid communities are more diverse and OTU-rich than their biofilm community counterparts, and mineral-hosted biofilm communities are more diverse than biofilm communities on inert controls ([Figure 4](#)).

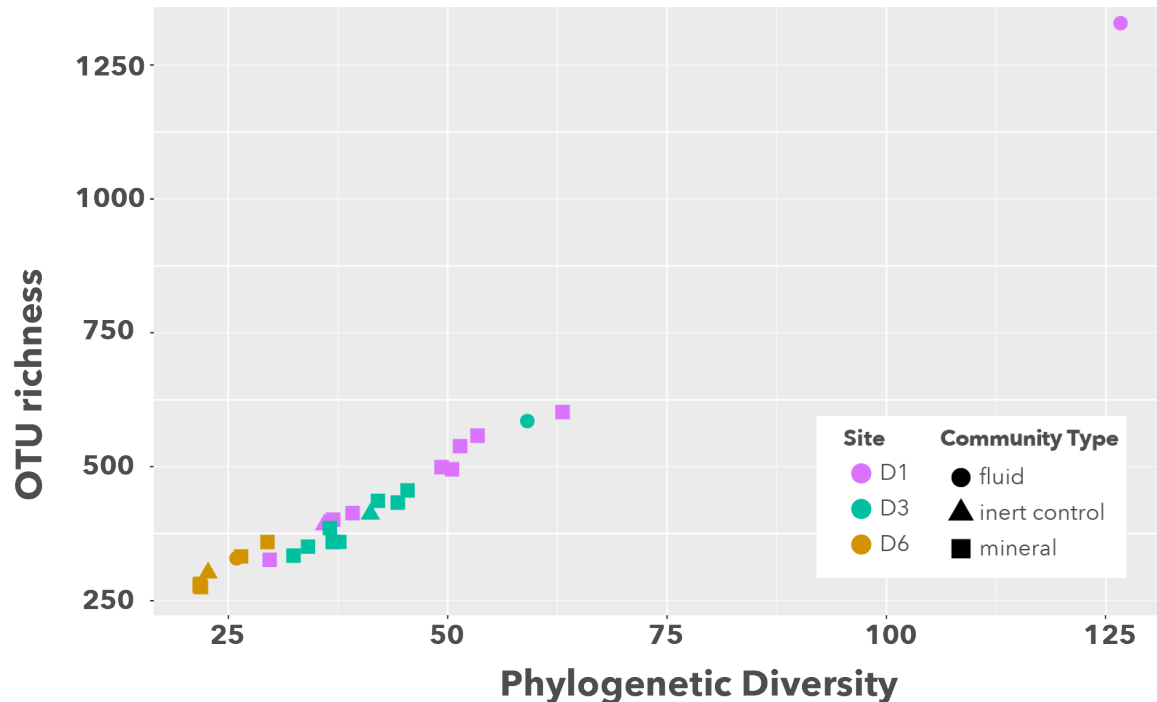


**Figure 4.** Alpha diversity of DeMMO fluid and biofilm communities.

DeMMO1 communities are dominated by members of *Nitrospirae*, *Omnitrophica*, *Betaproteobacteria*, and *Chloroflexi*, DeMMO3 by *Beta*-, *Delta*-, and *Alphaproteobacteria* and *Chloroflexi*, and DeMMO6 communities by *Delta**proteobacteria*, *Chloroflexi*, *Acetothermia*, and *Latescibacteria* (Figure 5). Broadly, members of the candidate phyla *Omnitrophica* are most enriched in fluid communities, whereas members of *Pseudomonadaceae*, *Rhodocyclaceae*, *Thermodesulfobacteriia*, and *Latescibacteria* are most enriched in biofilm communities. Members of *Desulfobulbaceae* and *Thermodesulfobacteriia* are highly enriched in mineral experiments relative to fluid communities, most notably in experiments with pyrolusite. NCBI BLAST results indicate that the *Desulfobulbaceae* in D3 communities on pyrolusite are dominated by an OTU with 92.89% similarity to a strain of *Desulfobulbus propionicus* capable of elemental sulfur disproportionation to sulfide (Pagani *et al.*, 2011). D6 communities are dominated by an OTU with 96.44% similarity to a strictly anaerobic strain of *Desulfobulbus elongatus* isolated from freshwater sediment capable of thiosulfate disproportionation to sulfite (Janssen *et al.*, 1996). The *Thermodesulfobacteriia* in D1 communities on pyrolusite are dominated by an OTU with 83.94% similarity to *Deferrisoma camini*, a thermophilic iron reducer isolated from a marine hydrothermal vent (Slobodkina *et al.*, 2012).

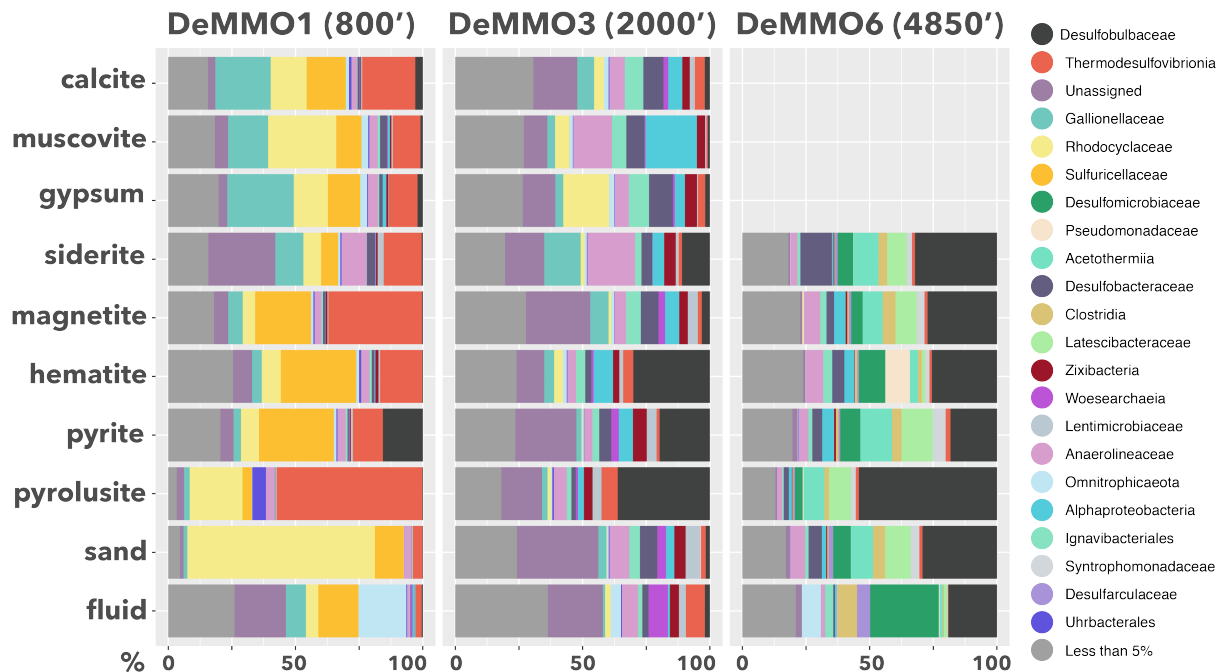


**Figure 5.** Beta diversity of DeMMO communities. Relative abundances of OTU's binned at the family level from selected DeMMO fluid and biofilm samples. Families that make up less than 5% of a community were binned as 'Less than 5%'.

### 3.3 | Mineral-hosted biomass

Scanning electron micrographs of biofilms reveal high variation in cell densities and morphologies. Generally, biofilm cell densities are 3-4 orders of magnitude greater than in fluid communities, and cell densities mineral-hosted biofilms are similar or lower than biofilms on inert controls on average (Figure 6). Overall, we observed the highest cell densities in D1 communities, and of these, the highest are in parallel control experiments. Of the minerals, we observed the highest cell densities on pyrolusite and lowest cell densities on calcite and muscovite. Generally, cell densities are higher on minerals than on internal controls, with exceptions being in D1 on pyrite and magnetite.

Biofilm morphologies differ markedly between experiments with pyrolusite and inert controls at D1 and D3. Inert controls are dominated by 0.2µm diameter bacilli and filaments, whereas biofilms on D1 pyrolusite are dominated by 0.2µm diameter bacilli and coccobacilli, and D3 pyrolusite by 3µm diameter coccobacilli and 0.5-1µm diameter bacilli, tapered stalks with hollow centers that sometimes bifurcate, and wire-like structures connecting cells and tapered stalks. Biofilms on D3 magnetite are dominated by 2µm diameter bacilli forming aggregates with local wire-like structures, where aggregates are comprised of randomly oriented cells or form unidirectional chains. Cells in D6 experiments with minerals are morphologically similar to those observed in experiments with inert controls; however, cell densities between experiment types differ by orders of magnitude.

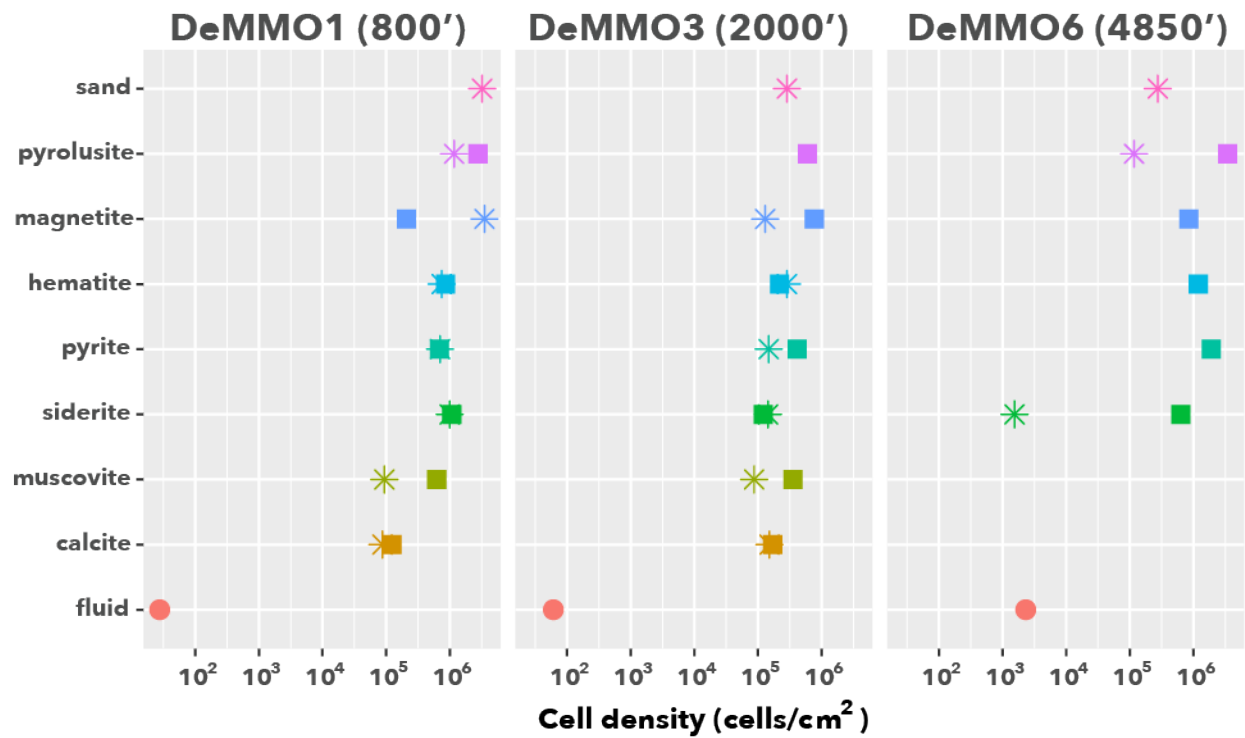


**Figure 6.** Averaged cell densities estimated from SEM images of glass slides and mineral coupons and filtered fluids. Minerals and fluids are denoted by squares and circles, respectively. Glass slides were included in experiments with minerals (internal inert controls) or sand (parallel inert controls), denoted by stars. Muscovite and calcite experiments were not installed at D6.

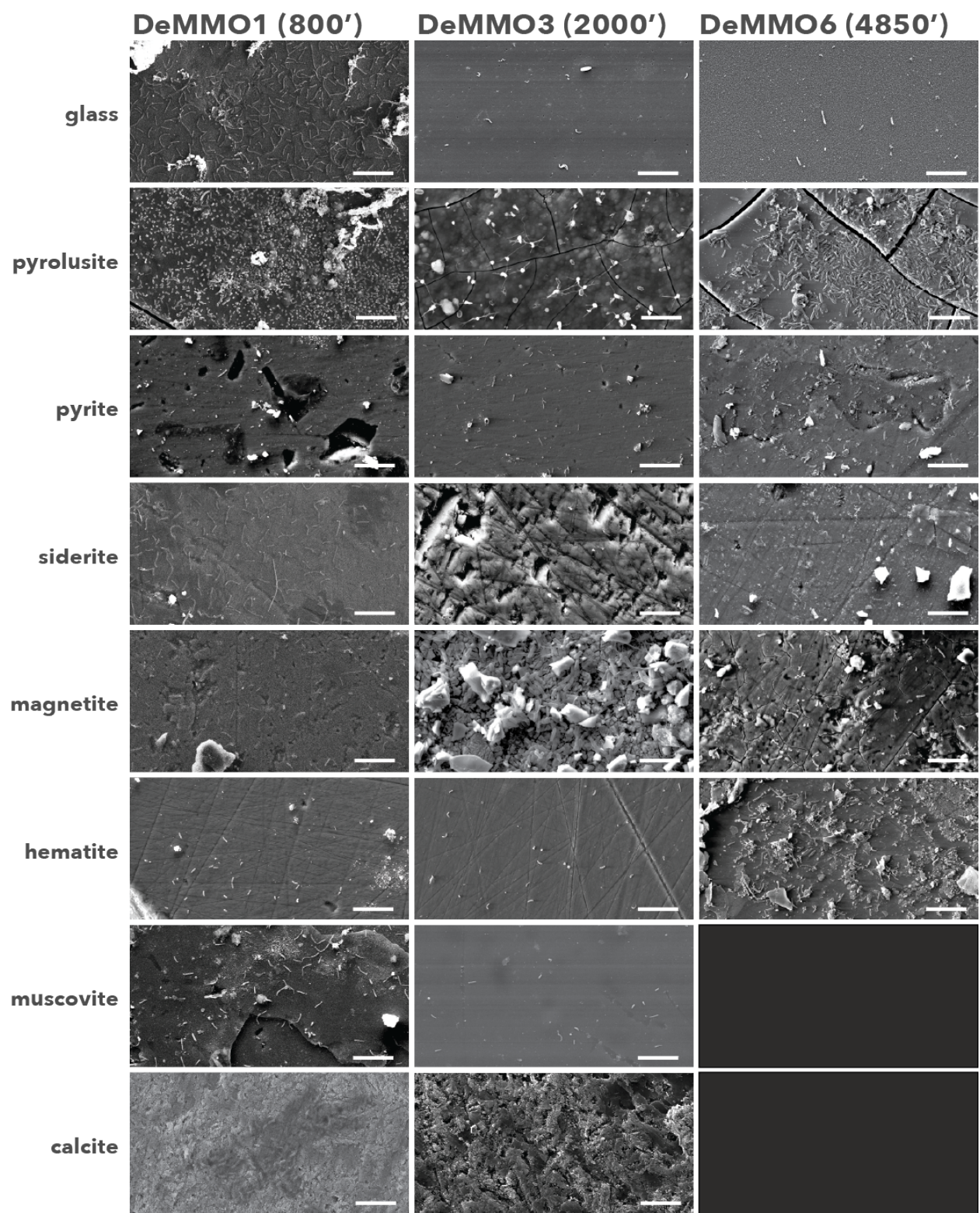


Figure 7. Biofilm communities on glass slides and mineral surfaces. Scale bars represent 10 $\mu$ m.

## 4 | DISCUSSION

### 4.1 Exergonic mineral metabolisms

Modeled metabolic reactions reveal that pyrite oxidation with nitrate is the most exergonic metabolism at DeMMO1, 3, and 6; however, energy density calculations, where limiting reactants are considered, indicate that nitrate is not as available for microbial metabolisms as other dissolved substrates. For example, pyrolusite reduction with carbon monoxide is a highly exergonic reaction and carbon monoxide is abundant, thus this metabolism may actually be more favorable in terms of energy density. Further, cell densities are consistently higher on pyrolusite than on pyrite, further supporting this idea. Given that all reactions with pyrolusite were exergonic at all three DeMMO sites, we expected results from experiments with pyrolusite to be distinct from experiments with other minerals. Indeed, our data suggest pyrolusite may enhance biofilm biomass and promote colonization by specific taxa at DeMMO which we discuss further here.

### 4.2 Microbial Communities

Generally, fluid communities are more taxonomically rich and phylogenetically diverse than their biofilm counterparts, suggesting specialists inhabit biofilm communities. Colonization by specialists may indicate only a subpopulation of the microbiome is capable of biofilm formation or using minerals as sources of energy. Alternatively, competition for dissolved substrates may promote mineral colonization by opportunists capable of taking advantage of energy available in minerals. Diversity has been shown to significantly increase within the first few days of biofilm development and remain relatively stable on timescales similar to our study (Gulmann *et al.*, 2015). We found no clear trends in diversity or biomass with duration of each experiment, which ranged from 80-231 days ([Supplementary Figure X](#)), suggesting the maturity of biofilms upon collection.

Microbial communities within each study location form distinct groups in NMDS space ([Figure 8](#)), suggesting that local environmental factors such as fluid geochemistry and host rock mineralogy are the primary drivers of dissimilarity among communities between each site, as shown previously (Osburn *et al.*, 2014). Further, DeMMO communities are compositionally distinct from ambient communities, indicating DeMMO communities are not majorly influenced by contamination ([Supplementary Figure X](#)). Additionally, NMDS ordination reveals differences between fluid and biofilm communities. While there is significant overlap among fluid and biofilm communities in NMDS space at D6, D1 fluid and biofilm communities are distinct. D1 communities shift from being dominated by *Omnitrophica* and Unassigned taxa in fluid communities to being dominated *Proteobacteria* and *Nitrospirae* in the biofilms. Many of the taxa enriched in D1 biofilms are well documented in biofilms in a variety of environments, including members of the *Gallionellaceae*, *Rhodocyclaceae*, and *Desulfobulbaceae* [[citations](#)]; therefore, it is unsurprising that an attached lifestyle may be favorable for these taxa at DeMMO. However, the lifestyles of candidate taxa dominant across DeMMO communities are not well documented elsewhere, and thus our experiments provide insight. Here *Omnitrophica* tends toward a free-living lifestyle, and *Uhrlbacterales* and *Latescibacteria* tend toward an attached lifestyle. Importantly, our experiments highlight the potentially significant differences than can exist between fluid and biofilm communities in the deep subsurface.

Several experiments with minerals enriched for biofilm communities distinct from fluid communities or biofilm communities on inert control substrates. Most striking are the experiments with pyrolusite, which hosted highly dense, morphologically distinct biofilm communities. These experiments enriched for members of the *Desulfobulbaceae* at DeMMO3 and DeMMO6 and *Thermodesulfovibrionia* at DeMMO1, suggesting mineral selectivity by these taxa. The closest relatives of the most dominant OTUs assigned to

these taxa were not found to be capable of MnO<sub>2</sub> reduction; however, ferric hydroxide was found to enhance the growth of *Desulfobulbus elongatus* (Janssen *et al.*, 1996). The presence of iron or manganese may indirectly stimulate growth of and promote mineral selectivity by sulfur reducing or disproportionating organisms by scavenging sulfide, a waste product of these metabolism (Thamdrup, 1993). Alternatively, pyrolusite selectivity may indicate that pyrolusite can be used as an energy source by these taxa. Relatives within the *Desulfobulbaceae* are capable of mineral reduction via extracellular electron transport (EET) (Pfeffer *et al.*, 2012), and we observed distinct wire-like structures on pyrolusite at D3 (Figure 9) that are visually similar to those produced by EET-capable organisms described elsewhere (Reguera *et al.*, 2005). These observations suggest the potential for preferential colonization of energy-yielding minerals by EET-capable taxa in deep subsurface biofilms.

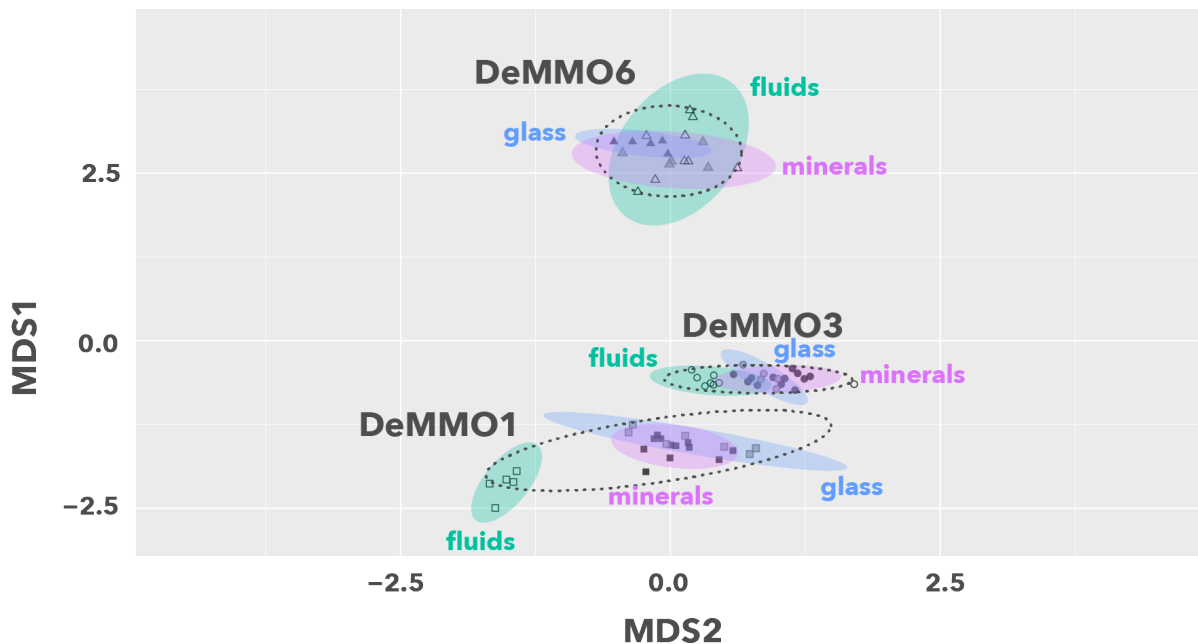


**Figure 8.** NMDS plot of DeMMO fluid and biofilm communities represented as hollow and filled points, respectively. 95% confidence ellipses encompass communities in each site (dotted), or fluid (green), mineral biofilm (purple) or control biofilm (blue) communities from each site.

#### 4.3 | Mineral-hosted biomass

Our estimates for fluid cell densities per square centimeter are conservatively high given our assumptions of a 100 $\mu\text{m}$  fracture width, where a width of 4-30 $\mu\text{m}$  may be more realistic (Murdoch *et al.*, 2012). Even with high fluid cell density estimates, we found that cell densities in biofilm communities are 3-4 orders of magnitude greater than in respective fluid communities. A potential driver of these differences in biomass observed between fluid and biofilm communities in the subsurface is host rock mineralogy. Mineral surfaces can promote biofilm colonization due to a variety of properties, including surface charge, conditioning films enhanced by mineral defects, enhanced nutrient concentration (Donlan, 2002; Flemming *et al.*, 2016), or energy availability as our coupled experimental and theoretical data suggest. Here, we found that cell densities were generally higher on mineral surfaces relative to inert controls at D3 and D6 by as much as 1-1.5 orders of magnitude, indicating that minerals can significantly enhance biomass in deep continental settings.

## 4 | CONCLUSIONS - Potential for a massive and diverse mineral-hosted deep biosphere

We successfully utilized *in situ* cultivation experiments to explore the role of minerals in driving differences in diversity and biomass between fluid and mineral-hosted microbial communities in a continental deep subsurface system. Here, variety of minerals are available as energy sources for microbial metabolisms; however, minerals may only be accessible to specialist taxa. We observed trends in community structure, cell densities, and biofilm morphologies that suggest mineral selectivity and potential for EET. We suggest our observations of biomass enhancement on energy-yielding minerals may be a result of mineral-stimulated metabolic activity. Biofilm formation on mineral surfaces may therefore offer a competitive advantage in this system, where continental rock rich in metal oxides under thermodynamically favorable conditions provides energy under otherwise energy-limited conditions. Thus, local host rock mineralogy has the potential greatly enhance biofilm biomass and drive significant differences in diversity between fluid and biofilm communities at DeMMO. Taken together, our findings suggest the capacity for a taxonomically distinct mineral-hosted deep subsurface biosphere of significant biomass at DeMMO, and by extension, host rock mineralogy is an important ecological driver in deep continental biospheres.

## ACKNOWLEDGEMENTS

This work was supported by NASA Headquarters under the NASA Earth and Space Science Fellowship Program – “Grant 80NSSC18K1267” and Exobiology Grant “...” and Northwestern University. We thank undergraduates Bethany Ketcham and Annamarie Jedziniak at Northwestern University for providing assistance with field work preparation and cell counts. We also thank Dr. Annette Rowe, Karla Abuyen, Dr. Haley Sapers, and the Sanford Underground Research Facility staff for assistance in the field. This work made use of the EPIC facility of Northwestern University’s NUANCE Center, which has received support from the Soft and Hybrid Nanotechnology Experimental (SHyNE) Resource (NSF ECCS-1542205); the MRSEC program (NSF DMR-1720139) at the Materials Research Center; the International Institute for Nanotechnology (IIN); the Keck Foundation; and the State of Illinois, through the IIN.

## References

- Bethke, C., & Yeakel, S. (2009). *Geochemist's Workbench: Release 8.0 Reaction Modeling Guide*. RockWare Incorporated.
- Jari Oksanen, F. Guillaume Blanchet, Michael Friendly, Roeland Kindt, Pierre Legendre, Dan McGlinn, Peter R. Minchin, R. B. O'Hara, Gavin L. Simpson, Peter Solymos, M. Henry H. Stevens, Eduard Szocs and Helene Wagner (2019). vegan: Community Ecology Package. R package version 2.5-4. <https://CRAN.R-project.org/package=vegan>
- Chaumeil PA, Mussig AJ, Hugenholtz P, Parks DH. 2019. GTDB-Tk: A toolkit to classify genomes with the Genome Taxonomy Database. <in prep>.

## Supplemental

- The OTU table and code used to perform statistical analyses and figs can be found at DOI: ..., github repo link

**Table 1.** Averaged fracture fluid geochemistry measured at three DeMMO sites between Dec. 2015 - Sep. 2018.

Site	Depth ft	Temp C°	ORP	pH	H2 nM	CO nM	CH4 nM	Fe <sup>2+</sup> mg/L	NH4 <sup>+</sup> mg/L	NO3 <sup>-</sup> mg/L	SO4 <sup>2-</sup> mg/L	S2 <sup>-</sup> µg/L	DOC mg/L	DIC mM
D1	800	10.3	-86.8	7.2	0.12	0.2	0.48	2.4	0.1	0.3	336.1	1.7	0.43	4.2
D3	2,000	16.2	-34.5	7.1	0.27	0.3	4.29	2.5	0.2	0.3	1674.2	10.1	0.25	10.0

D6	4,850	21.5	-236.2	8.1	0.30	0.1	314.3	1.2	0.1	0.3	4223.3	66.2	0.25	2.2
----	-------	------	--------	-----	------	-----	-------	-----	-----	-----	--------	------	------	-----

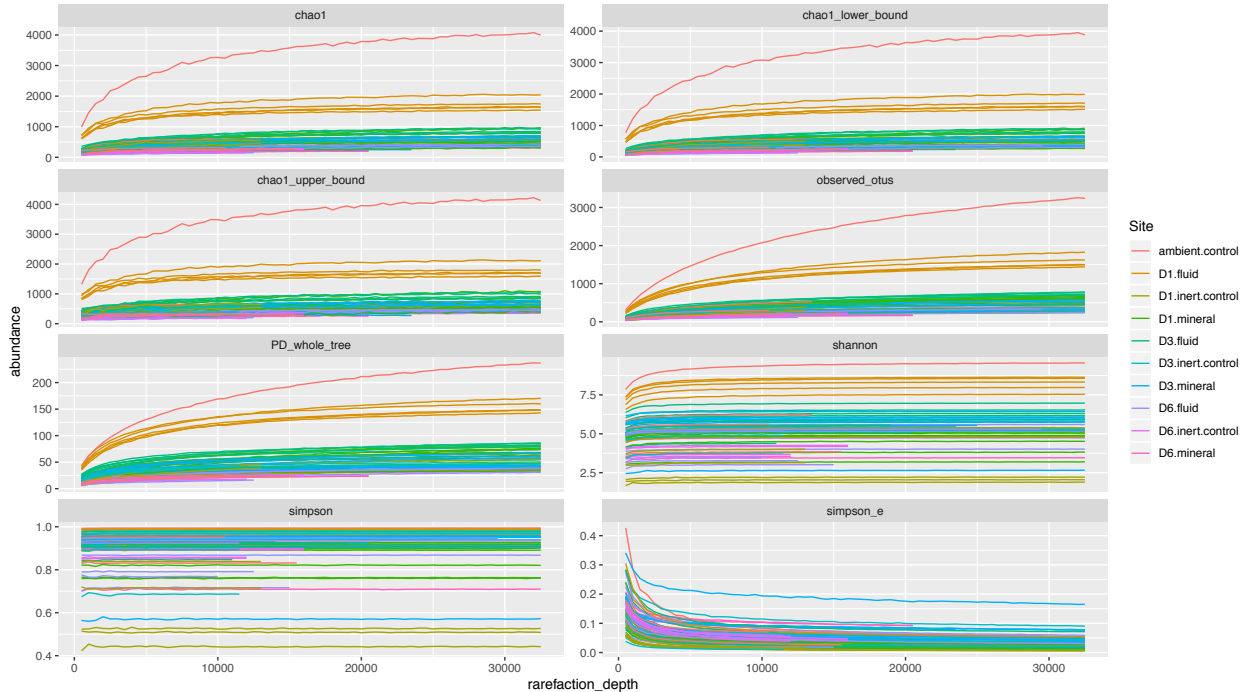


**Figure x.** Alpha diversity of DeMMO communities. Rarefaction curves illustrate the number of OTU observations across a range of sequencing depths.

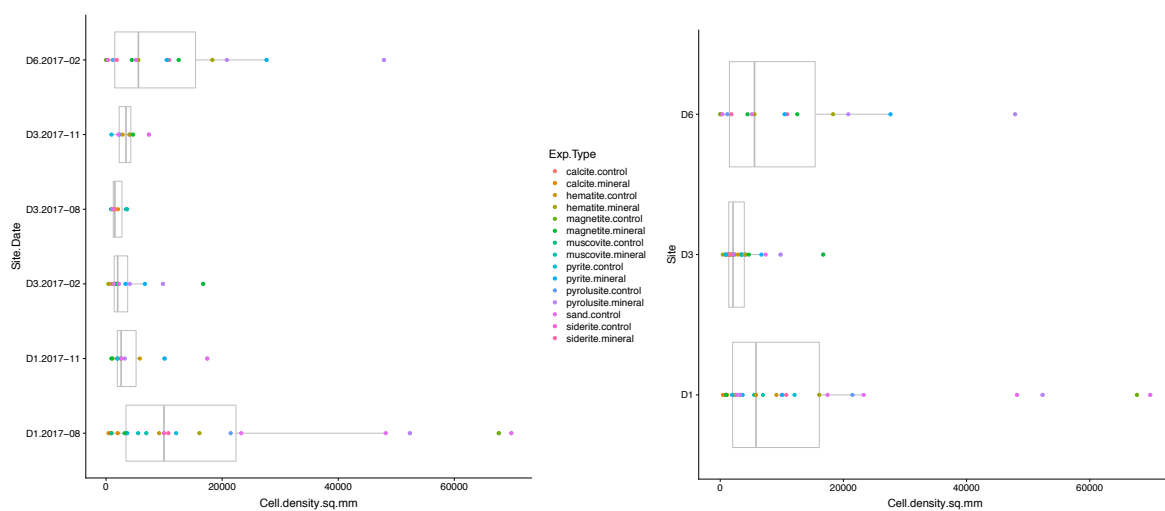


**Figure x.** Left: Cell densities vs. sampling date for each site. Right: Cell densities vs. site over all sampling dates.

Figure X. NMDS including ambient controls

Figure X. bar plot with dendrogram for all communities

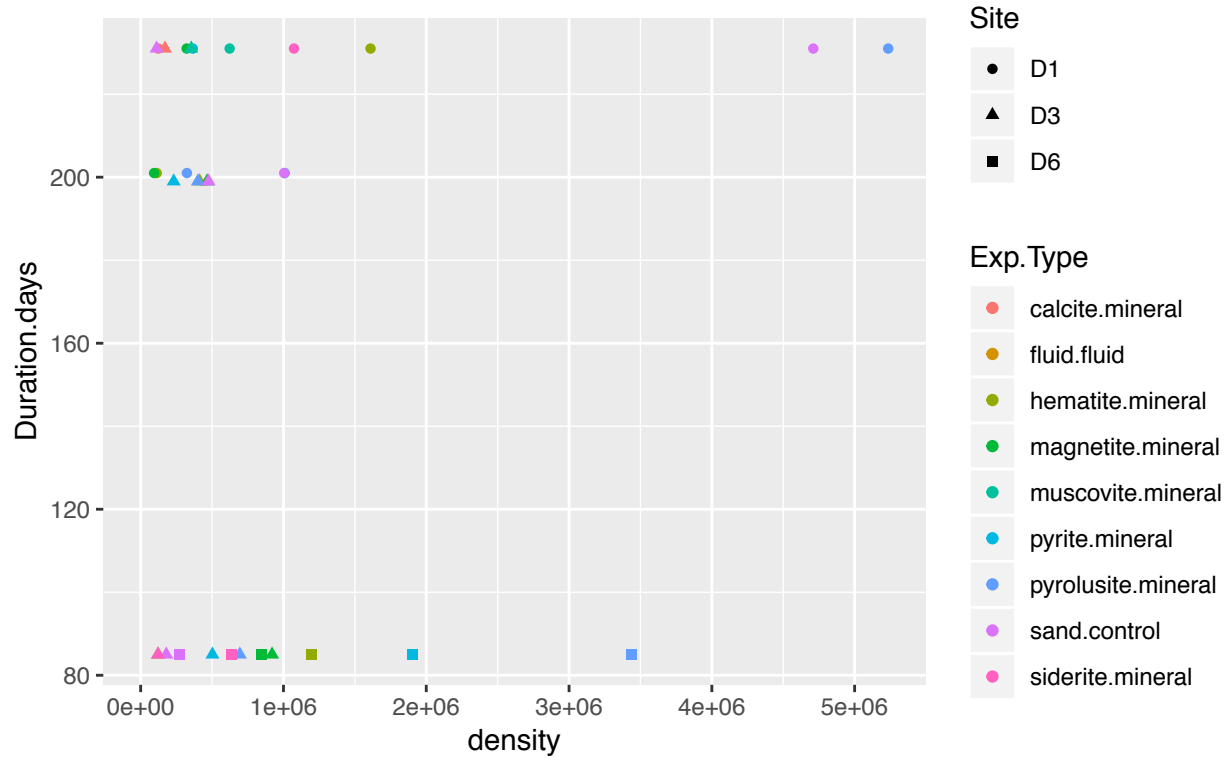
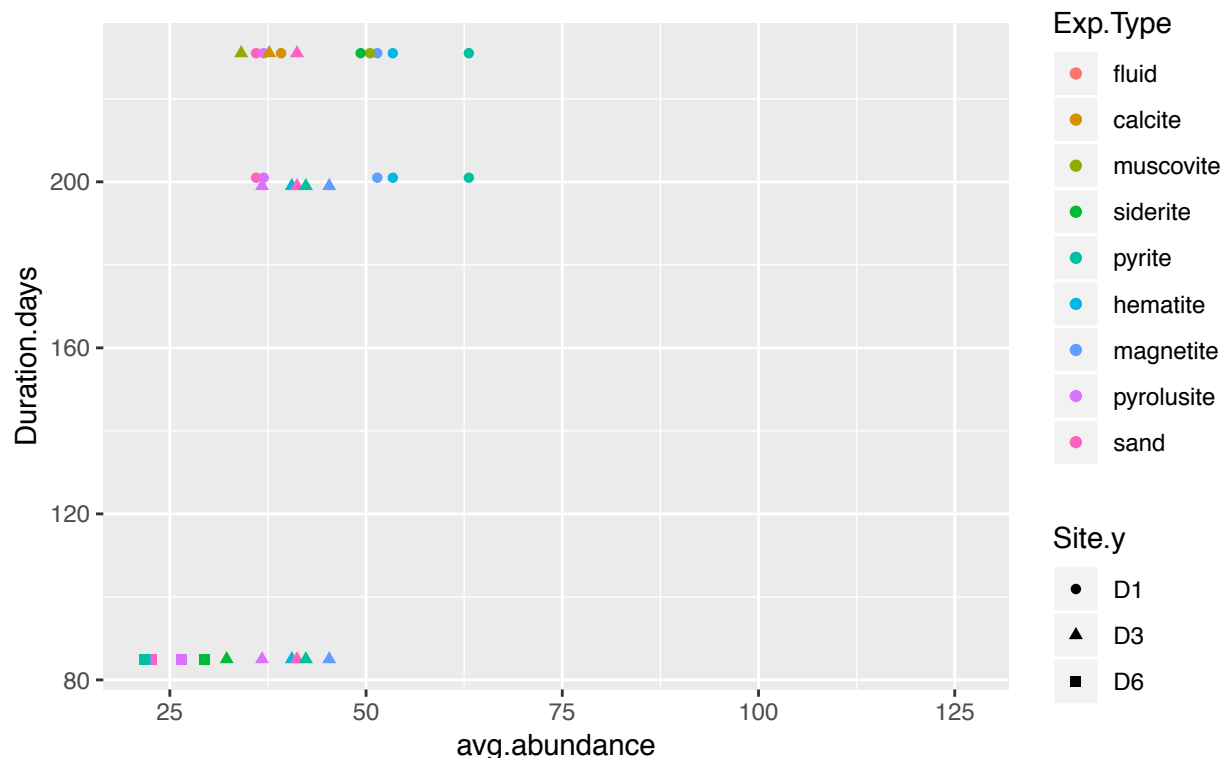


Figure x. Cell densities vs. duration of each experiment.



**Figure x.** Phylogenetic diversity vs. duration of each experiment.